CHAPTER 1

On parameterizations of air–sea fluxes

W.M. Drennan
Division of Applied Marine Physics, Rosenstiel School of Marine and Atmospheric Science, University of Miami, USA.

Abstract

In order to understand and model many physical processes relating to the atmosphere and ocean, it is necessary to consider how the two are coupled. The air–sea fluxes of momentum, heat, and mass are the key quantities linking the two fluids. However, since fluxes over the sea are difficult and costly to measure, especially over the time and space scales required for model input, they have long been parameterized in terms of more readily available mean parameters and bulk exchange coefficients.

In this paper we review the present state of the art of parameterizing air–sea turbulent fluxes. A data set of eddy-correlation fluxes compiled during eight field experiments, and representing a wide range of conditions, is used to investigate traditional bulk flux parameterizations (i.e. wind-speed dependent momentum coefficients, constant sensible and latent heat coefficients), as well as several more recent algorithms. Particular emphasis is given to the effect of sea state on the fluxes.

1 Introduction

Over the past decades, our ability to model the global environment has improved considerably. This is not only due to vastly superior computer resources but also due to a better understanding of many of the physical processes. The focus of recent years has been on the longer term, i.e. climate models (Shindell *et al.* [1]), and also extreme events, such as hurricanes (Bao *et al.* [2]). In both cases, progress relies on treating the atmosphere and ocean as a coupled system, taking into account exchanges at the air–sea interface. Here we focus on the turbulent exchanges, referring the reader elsewhere (e.g. Garratt [3]) for information on radiative transfers.

WIT Transactions on State of the Art in Science and Engineering, Vol 23, © 2006 WIT Press
www.witpress.com, ISSN 1755-8336 (on-line)
doi:10.2495/978-1-85312-929-2/01

Turbulence at the air–sea interface is generated primarily by two mechanisms: buoyancy and shear, the latter generated by the roughness at the air–sea interface. The sea surface is characterized by waves with wavelengths ranging over five orders of magnitude, from centimeter scale ripples to ocean swells hundreds of meters long. The composition of the wave field varies with time and space primarily according to the surface wind field and its history, and also surface currents, air and sea temperatures, and, near the coast, bathymetry. The air–sea interface is fundamentally different from the air–land interface in that the roughness elements are mobile, and evolve with both the atmosphere and the ocean. The waves grow by extracting momentum from the air through pressure–slope correlations. As a wave field develops, the surface roughness changes, which in turn affects the turbulent momentum transfer. The waves and atmospheric boundary layer represent a truly coupled system.

Since air–sea fluxes are the boundary conditions for both the atmosphere and the ocean, knowledge of them at suitable spatial and temporal scales is important. However, direct measurement of these fluxes over the sea is difficult and expensive, and hence measured fluxes are rarely available. Instead, models rely on parameterized fluxes, based on more easily measured mean variables such as wind speed, air and sea temperatures, etc. The development of accurate flux parameterizations has been a goal of air–sea interaction research for many decades. Flux parameterizations have progressed well beyond the early efforts where the bulk transfer coefficients were assumed to be constants.

Here we assess the present state of air–sea turbulent flux parameterizations, with particular attention paid to the effects of sea state. We start by summarizing some of the theory underlying boundary layer turbulence (Section 2). We then introduce an extensive data set combining turbulent flux and wave measurements from a wide variety of conditions (Sections 3 and 4), and use it to study the effect of sea state on the momentum (Section 5) and heat fluxes (Section 6). Finally, we discuss limitations to our current knowledge, with particular emphasis on the high wind regime (Section 7).

2 Turbulent fluxes and the Monin–Obukhov similarity theory

The turbulent fluxes of momentum, sensible heat, and mass are given by

$$\vec{\tau} = \rho(-\overline{w'u'}\hat{i} - \overline{w'v'}\hat{j}), \tag{1a}$$

$$H = \rho C_P \overline{w'\theta'}, \tag{1b}$$

and

$$M_X = \rho\overline{w'x'}, \tag{1c}$$

respectively, where the primes indicate turbulent fluctuations, u, v, w, and θ represent up-wind velocity, cross-wind velocity, vertical velocity, and potential temperature, respectively, x is the mixing ratio of some constituent with respect to dry air,

ρ is the air density, C_P is the specific heat at constant pressure, and the overbars represent averages over a time period of $O(20\,\text{min})$.

The mass fluxes of particular current interest are those of humidity q, and carbon dioxide. Although eqn (1c) is written in terms of the mixing ratio, typical sensors measure the mass concentration, $c = \rho x$. Webb *et al.* [4] show that if the mass concentration is used in eqn (1c), a correction must be made to account for the fluctuations in ρ caused by temperature and water vapor. The second order correction is given by

$$M_X = \overline{w'c'} - \bar{c}T_{\text{v}}^{-1}\overline{w't'_{\text{v}}}, \tag{2}$$

where the virtual temperature $t_{\text{v}} = \theta(1+0.61r)$, where r is the mixing ratio of water vapor in dry air. The upper case variables (T_{v}, U, etc.) refer to mean quantities. For CO_2 flux, the Webb correction is very important, being of the same order as the measured flux (Fairall *et al.* [5]). For water vapor, the Webb correction is small, typically several percent, and is usually neglected. The latent heat flux E is related to the humidity flux M_q by $E = L_{\text{v}}M_q$, where L_{v} is the latent heat of vaporization.

Efforts to model the turbulent exchange rely on the ideas of flow similarity, as proposed by Monin and Obukhov [6]. Under the assumptions of stationarity and homogeneity, it can be shown (Busch [7]) that the heat flux is constant with height and that the vertical gradient of the momentum flux is balanced by Coriolis terms. Close to the surface, typically taken as the lower 10% of the boundary layer, the effect of the Coriolis terms is small, and the momentum flux is usually assumed to be constant with height. Although the error associated with this constant-flux assumption is small near the surface, it increases linearly with height. It is clearly significant for most aircraft measurements, and may also be at the 20 m measurement heights typical of ships. Hence the correction of Donelan [8] should be applied.

Within the "constant" flux layer, one can define the turbulence scaling parameters,

$$u_* = (|\tau|/\rho)^{1/2}, \quad t_* = -(H/\rho C_P)/u_* \quad \text{and} \quad x_* = -(M_X/\rho)/u_*, \tag{3}$$

for momentum, heat, and mass, respectively. u_*, defined in eqn (3), is known as the friction velocity. Then, assuming that turbulence in the surface layer is generated by a combination of surface shear and buoyancy (this neglects the region very near the surface, where molecular processes are also important), the Monin–Obukhov (MO) theory asserts that the mean gradients and scaling parameters are related through universal dimensionless gradient functions Φ of the form:

$$\frac{\partial U}{\partial z} = \frac{u_*}{\kappa z}\Phi_u\left(\frac{z}{L}\right); \frac{\partial \Theta}{\partial z} = \frac{t_*}{\kappa z}\Phi_\theta\left(\frac{z}{L}\right); \frac{\partial X}{\partial z} = \frac{x_*}{\kappa z}\Phi_x\left(\frac{z}{L}\right), \tag{4}$$

where z is the mean height above the surface, and L is the Obukhov length,

$$L = -u_*^3[\kappa g(H/(C_P\Theta) + 0.61E/L_{\text{v}})/\rho]^{-1} = -u_*^3[\kappa F_{\text{B}}]^{-1}, \tag{5}$$

where F_{B} is the buoyancy flux, $\kappa \approx 0.4$ is the von Kármán constant, and g is the gravitational constant. The Obukhov length represents the height where turbulence production due to shear is equal to that due to buoyancy.

Integrating eqn (4) from the surface to some height z in the constant flux layer gives

$$\frac{U(z)-U(0)}{u_*}=\frac{\Phi_u(0)}{\kappa}\left[\log\left(\frac{z}{z_0}\right)-\Psi_u\left(\frac{z}{L}\right)\right], \tag{6a}$$

$$\frac{\Theta(z)-\Theta(0)}{t_*}=\frac{\Phi_\theta(0)}{\kappa}\left[\log\left(\frac{z}{z_{0t}}\right)-\Psi_\theta\left(\frac{z}{L}\right)\right], \tag{6b}$$

$$\frac{X(z)-X(0)}{x_*}=\frac{\Phi_x(0)}{\kappa}\left[\log\left(\frac{z}{z_{0x}}\right)-\Psi_x\left(\frac{z}{L}\right)\right], \tag{6c}$$

where z_0, z_{0t}, and z_{0x} are the surface roughness lengths for momentum, heat, and mass (i.e. the heights where the profiles cross zero). The functions Ψ in eqn (6) are related to the integrated flux profile or gradient relations Φ. Recent data support $\Phi_u(0)=1$, while values of 0.85 (Donelan [8]) and 0.95 (Högström [9]) have each been recommended for $\Phi_\theta(0)=\Phi_x(0)$. Note that it is common to replace $\Phi_\theta(0)$ and $\Phi_x(0)$ in eqn (6) by the turbulent Prandtl number, $\mathrm{Pr}=\Phi_\theta(0)/\Phi_u(0)=\Phi_x(0)/\Phi_u(0)$.

In neutral conditions, where buoyant forcing becomes negligible, $|z/L|\to 0$, and the Ψ functions approach zero. Equation (6) then yields the well-known logarithmic forms,

$$\frac{U_{\mathrm{N}}(z)-U(0)}{u_*}=\frac{1}{\kappa}\log\left(\frac{z}{z_0}\right), \tag{7a}$$

$$\frac{\Theta_{\mathrm{N}}(z)-\Theta(0)}{t_*}=\frac{\mathrm{Pr}}{\kappa}\log\left(\frac{z}{z_{0t}}\right), \tag{7b}$$

$$\frac{X_{\mathrm{N}}(z)-X(0)}{x_*}=\frac{\mathrm{Pr}}{\kappa}\log\left(\frac{z}{z_{0x}}\right), \tag{7c}$$

where the subscript N represents neutral conditions.

Since the introduction of MO theory, considerable work has been carried out to determine the dimensionless gradient functions. Early experimental verification of MO similarity in the atmosphere over land was given by Zilitinkevich and Chalikov [10], Dyer and Hicks [11], and Businger *et al.* [12]. Although there is some scatter between the various data sets and the resultant profile functions, Högström [9, 13] found the various forms to be consistent within 10–20% within the region $|z/L|<0.5$.

The first systematic investigations of the equivalent problem in the marine environment were made around the same time. In general, flux measurements over the ocean showed good spectral agreement with the terrestrial measurements (e.g. Miyake *et al.* [14]; Pond *et al.* [15]). An exception was found in the presence of swell where upward momentum fluxes were occasionally noted (Volkov [16]; Makova [17]). Likewise, Holland *et al.* [18] reported negative wind speed gradients (larger winds near the surface) in swell conditions.

Pond *et al.* [15], Paulson *et al.* [19], and Davidson [20] presented simultaneous measurements of fluxes, profiles, and surface waves from the FLIP platform during the BOMEX experiment. These data show general support for the MO theory. However, as the motion of the platform was not measured, it was not possible to separate wave-induced motion of the platform from a possible wave-coherent signal in the velocity components: all anomalous signals in the motion band were filtered out. Although necessary at the time, a consequence of this is the loss of wave-coherent information (crucial for the study of wave effects). To summarize, most early experiments, except for some carried out in swell-dominated conditions, were seen to support MO theory over water, with most data indicating general support for the land-based stability functions.

3 Measuring turbulent fluxes

3.1 Direct methods

The calculation of fluxes via eqn (1) requires the measurement of the turbulent fluctuations of vertical velocity w', along with u', v', θ', and x'. This direct calculation of fluxes is referred to as the "eddy correlation" or "direct covariance" method. Sampling of the turbulent signals must be fast enough, and for a sufficiently long period, to capture all scales contributing to the flux. Based on the universal cospectral shapes of Kaimal *et al.* [21], in neutral conditions 95% of the cospectral energy of momentum (heat) is contained in the dimensionless frequency range 0.0018 (0.0024) $< fz/U <$ 1.3 (2.5), where f is the frequency [Hz]. Consequently, for typical measurement heights and wind speeds, sampling frequency and time series length of orders 10 Hz and 20 min, respectively, are recommended. The sampling length should be increased if strongly unstable conditions ($z/L \ll 0$) are expected, and may be reduced in very stable conditions. Sampling lengths in excess of O(60 min) are not recommended due to the influence of mesoscale effects which do not contribute to the turbulent fluxes. See Mahrt *et al.* [22] for a discussion of this and other flux sampling issues.

Although common over land, direct flux measurements over the sea have been limited by both the mobility and the bulkiness of typical marine platforms. Flux towers are relatively rare in the marine environment, being limited by design constraints to the coastal regions. Instead, fluxes are usually measured from ships, buoys, or aircraft, all mobile platforms. The technology for measuring fluxes from aircraft was developed during the 1960s. Such measurements rely on nose-mounted gust or pressure probes, with corrections for aircraft motion as measured by an inertial platform (e.g. Axford [23]). With the development of compact and inexpensive rate gyros and accelerometers, similar systems have been developed for use on buoys (Anctil *et al.* [24]) and ships (Edson *et al.* [25]). Consequently, the problems associated with platform mobility have essentially been solved.

The second limitation is more serious. Flow distortion, a concern with all turbulence measurements (Wieringa [26]; Wyngaard [27]), can be particularly bad over

the sea, where platforms must be designed to survive the hostile marine environment. In considering flow distortion the mean and turbulent components of the flow field are usually considered separately. The effects of mean flow distortion can be assessed through numerical (turbulence closure) models using commercial software (e.g. Yelland *et al.* [28]; Dupuis *et al.* [29]) or flume studies using scale models. Mean flow distortion is characterized by the lifting, tilting, and compression of flow streamlines as they pass over or around the platform. The results of Dupuis *et al.* [29] for flow around the 85 m vessel *L'Atalante* are typical: for moderate, bow-on winds, the flow at the top of a 17 m mast near the bow was decelerated by 8%, tilted upward by $\sim 7°$, and uplifted by 1.2 m. The effects vary with wind speed and direction, with the distortion increasing significantly for flow angles greater than 30° relative to the bow.

The effect of distortion of the turbulent components remains beyond the reach of current numerical models, and is therefore more difficult to assess. Recent studies comparing turbulent fluxes measured on large ships with those from nearby buoys (which are assumed to be largely free of flow distortion effects) indicate a good comparison between scalar fluxes, but an enhancement of the ship-board momentum flux by an order of 15% (Edson *et al.* [25]; Pedreros *et al.* [30]). It is expected that agreement is better in conditions with low ship motion, and will worsen if considerable slamming is experienced.

3.2 Indirect methods—inertial dissipation

The "inertial dissipation" (ID) method was used by Pond *et al.* [15] as a means to avoid the problems of ship motion and turbulent flow distortion. For momentum flux, the method is derived from the turbulent kinetic energy (TKE) conservation equation which for stationary and horizontally homogeneous conditions is:

$$u_*^2 \frac{\partial U}{\partial z} + F_B - \frac{\partial}{\partial z}\overline{w'e'} - \frac{1}{\rho}\frac{\partial}{\partial z}\overline{w'p'} - \varepsilon = 0, \tag{8}$$

where $e' = (u'^2 + v'^2 + w'^2)/2$ and p' represent fluctuations in TKE and pressure, respectively, and ε is the TKE dissipation rate. The terms in eqn (8) are, respectively, production of TKE from shear, production (or loss) due to buoyancy, transport of TKE, pressure transport, and loss due to dissipation. Similar expressions based on scalar variance budgets exist for the scalar fluxes (e.g. Large and Pond [31]).

Dividing eqn (8) by $u_*^3/\kappa z$ we arrive at

$$\Phi_u - \zeta - \Phi_e - \Phi_p - \frac{\kappa z}{u_*^3}\varepsilon = 0, \tag{9}$$

where

$$\Phi_e = \frac{\kappa z}{u_*^3}\frac{\partial \overline{w'e'}}{\partial z} \quad \text{and} \quad \Phi_p = \frac{\kappa z}{\rho u_*^3}\frac{\partial \overline{w'p'}}{\partial z}.$$

Using the assumptions of MO theory, the terms in the above equation are expected to be universal functions of $\zeta = z/L$. Then from a known dissipation rate and known

dimensionless functions (e.g. those of Högström [13]), the stress can be readily determined. In practice, ε is usually estimated from the inertial subrange (ISR) of the frequency spectrum, assuming Taylor's hypothesis:

$$\varepsilon = \left(\overline{f^{5/3}S(f)}/\alpha_{\mathrm{K}}\right)^{3/2} (2\pi/U_{\mathrm{a}})\,, \tag{10}$$

where $S(f)$ is the velocity spectrum, and the mean is taken over frequencies in the ISR, where $S(f) \propto f^{-5/3}$. Here $\alpha_{\mathrm{K}} \approx 0.52$ is the Kolmogorov constant and U_{a} is the advection velocity of turbulence past the probe. This dependence only on ISR frequencies ($f >\sim 2\,\mathrm{Hz}$) is the key advantage of the ID method. These high frequencies are unaffected by either turbulent (but not mean) flow distortion or platform motion. Hence the method remains popular for flux measurements from vessels (e.g. Yelland *et al.* [28]).

With little experimental data available on either $\bar{\Phi}_e$ or especially $\bar{\Phi}_p$, they are usually combined as a single transport (or imbalance) term $\bar{\Phi}_t = \bar{\Phi}_e + \bar{\Phi}_p$. This term is then either assumed to be zero (Large and Pond [32]) or determined empirically (Dupuis *et al.* [33]). See Sjöblom and Smedman [34] for a critical assessment of these assumptions in marine boundary layers.

Equation (9) can be rewritten to yield the expression for u_*:

$$u_* = [\kappa z\varepsilon/(\Phi_u(\zeta) - \zeta - \Phi_t(\zeta))]^{1/3}\,. \tag{11}$$

The ID heat flux is given by $\overline{w'\theta'} = [\kappa z\, u_*\, \varepsilon_\theta/\Phi_\theta(\zeta)]^{1/2}$, where $\varepsilon_\theta = \left(\overline{f^{5/3}S_\theta(f)}/\alpha_\theta\right) \varepsilon^{1/3}\,(2\pi/U_{\mathrm{a}})^{2/3}$. Here the Obukhov–Corrsin constant $\alpha_\theta \approx 0.8$. Expressions are similar for other scalar fluxes (Dupuis *et al.* [29]).

Given the assumptions underlying the ID method, its applicability has been questioned in certain conditions, namely in developing seas (Janssen [35]; but see also Taylor and Yelland [36]), in swell-dominated conditions (Donelan *et al.* [37]), and in light winds (Yelland *et al.* [28]). However, in the mixed seas typical of the open ocean ID fluxes compare well with direct measurements (Dupuis *et al.* [29]).

3.3 Indirect methods—profile

The profile method uses the dimensionless gradient functions (4), along with measured profiles, to estimate u_*, t_*, q_*, etc., and therefore, via eqn (3), the fluxes. The method is rarely employed over the sea, as profile measurements from vessels are particularly prone to mean flow distortion errors, since the flow distortion around a vessel is itself a function of height. Nevertheless, the recent profile measurements of CO_2 flux by McGillis *et al.* [38] are consistent with simultaneous direct flux measurements.

3.4 Indirect methods—bulk

Bulk fluxes are not measured fluxes, but estimates of fluxes derived from measured mean variables along with empirical bulk coefficients. Bulk transfer coefficients

relate the turbulent fluxes through the scaling parameters (3) to the more easily measured mean quantities U, Θ, and X, at the surface (subscript 0), and at some height above the surface. For momentum (the drag coefficient C_{D}), sensible heat (Stanton number C_{H}), and mass (constituent x, C_X), the z-m bulk relations are:

$$C_{\mathrm{D}}(z) = |\tau/\rho| \,/(U_z - U_0)^2 = (u_*/(U_z - U_0))^2, \tag{12a}$$

$$C_{\mathrm{H}}(z) = -\overline{w'\theta'}/\left[(\Theta_z - \Theta_0)(U_z - U_0)\right], \tag{12b}$$

$$C_X(z) = -M_x/\left[\rho(X_Z - X_0)(U_Z - U_0)\right]. \tag{12c}$$

For humidity, the bulk mass coefficient is known as the Dalton number, C_{E}.

Given the difficulty of measuring fluxes at sea many flux applications, particularly those requiring dense spatial information, such as atmospheric or climate modeling, rely on bulk fluxes. Consequently, considerable efforts have been expended over the past decades in determining accurate bulk parameterizations. A summary of recent efforts is found in Brunke *et al.* [39].

It follows from eqns (7) and (12) that the neutral z-m bulk coefficients are directly related to the surface roughness lengths, i.e. $C_{\mathrm{DN}}(z) = f(z/z_0)$. Based on dimensional reasoning, Charnock [40] proposed that $z_0 = \alpha u_*^2/g$, where α is known as the Charnock parameter. Charnock took α as a constant, which implies $C_{\mathrm{DN}}(z) = f(z, U_{\mathrm{N}}(z))$. Mean experimental values of α lie in the range 0.011–0.018 (Kraus and Businger [41]).

Henceforth, we consider the bulk coefficients evaluated at the standard reference height z of 10 m, i.e. $C_{\mathrm{D10N}} = f(U_{\mathrm{10N}})$, although for convenience the subscript 10 is usually omitted. This form of the bulk coefficients has been studied for decades, and many different relationships have been determined (see Geernaert [42]). However, it is now evident that no single parameterization of this type is able to adequately model all data sets, nor to describe the variability (beyond sampling error, cf. Sreenivasan *et al.* [43]) within most data sets. One goal here is to determine whether, and under what conditions, such bulk relationships are valid. We first introduce the data sets we will use.

4 Field data

The data sets, listed in Table 1, include a wide range of conditions from open ocean to near-shore. Each data set includes eddy correlation measurements of momentum flux along with mean meteorological and sea state parameters.

Three of the experiments are tower based: the Water Air Vertical Exchange Study (WAVES), 1 km off shore in Lake Ontario (Donelan *et al.* [44]; Drennan *et al.* [45]); the Risø Air–Sea Exchange experiment (RASEX), in the Baltic Sea, 2 km offshore (Johnson *et al.* [46]); Humidity Exchange Over the Sea experiment (HEXOS), 9 km offshore in the North Sea (Smith *et al.* [47]; DeCosmo *et al.* [48]). Although HEXOS was focused on humidity flux measurements, these data are not readily available. We use here only the momentum flux data as tabulated by Janssen [49].

Table 1: Summary of field data used in this paper.

Experiment	Reference	Location	Dates	Platform	Depth (m)	No. of runs (WSD)	Avg. (min)	U (m/s)	Fluxes
AGILE	[50]	Lake Ontario	1995–1996	Ship	4–50	101 (82)	20–30	3–15	U, T, Q, C
AWE		Coastal Atlantic	2000	Buoy	20	565 (335)	60	2–13	U, T_s
FETCH	[53]	Mediterranean Sea	1998	Buoy	100	853 (323)	28	2–19	U, T_s
GASEX	[55]	Pacific Ocean	2001	Buoy	4000	456 (0)	30	3–11	U, T, Q, C
HEXOS	[49]	North Sea	1986	Tower	18	50 (50)	20	9–20	U, Q
RASEX	[46]	Baltic Sea	1994	Tower	4	80 (80)	30	4–16	U
SWADE	[37]	Coastal Atlantic	1991	Ship	20–1000	122 (43)	17	4–14	U, T, Q
WAVES	[45]	Lake Ontario	1987	Tower	12	238 (156)	30	2–16	U

The quantities in brackets in the "No. of runs" column refer to the number of wind sea dominant (WSD) runs. The column "Avg." gives the average time for calculating the fluxes. The symbols in the "Fluxes" column refer to the availability of fluxes of momentum (U), sensible heat (T), humidity (Q), virtual or sonic temperature (T_s) and CO_2 (C).

WIT Transactions on State of the Art in Science and Engineering, Vol 23, © 2006 WIT Press
www.witpress.com, ISSN 1755-8336 (on-line)

Two other data sets are from small ships: the 15 m R/V *Agile* in Lake Ontario (Donelan and Drennan [50]) and the 20 m SWATH ship R/V *Frederick G. Creed* during the Surface Wave Dynamics Experiment (SWADE), in the coastal Atlantic (Katsaros *et al.* [51]; Donelan *et al.* [37]). Both ships were equipped with fast response dry- and wet-bulb thermocouples, as well as anemometers, yielding momentum, sensible heat, and moisture fluxes. The *Agile* also carried a LICOR 6262 closed path infrared gas analyzer, allowing for the calculation of CO_2 flux.

The remaining data sets were collected during several recent deployments of Air–Sea Interaction Spar (ASIS) buoys (Graber *et al.* [52]). Of these deployments, only FETCH (a French acronym for fluxes, sea state and remote sensing in variable fetch conditions) in the Mediterranean Sea has been described elsewhere (Drennan *et al.* [53]); the other two will be summarized briefly here.

The Adverse Weather Experiment (AWE), took place off Florida's Atlantic coast, during April–May 2000. The goal of AWE was to investigate the impact of adverse weather fronts on mixing and air–sea interaction in the shallow water column. The principal measurements during the experiment were TKE dissipation rates from an autonomous underwater vehicle (Dhanak *et al.* [54]), surface currents from an Ocean Surface Current Radar, and air–sea fluxes of momentum and buoyancy, along with surface waves, from an ASIS buoy. The ASIS flux measurements were taken using a Gill R2A sonic anemometer mounted at 7 m above mean sea level. The ASIS buoy was moored at 20 m depth, 2 km from the coast, usually just inshore of the Gulf Stream.

During February 2001, an ASIS buoy was deployed as part of the GASEX experiment which focused on air–sea CO_2 exchange in the equatorial Pacific (McGillis *et al.* [55]). In this Lagrangian study, the ASIS buoy was drogued and drifted in the South Equatorial Current. The air–sea fluxes of momentum, heat, water vapor, and CO_2 were measured from ASIS buoys (and from the R/V *Ronald H. Brown*) using Gill R2A sonic anemometers and LICOR-7500 open-path gas analyzers (for CO_2 and H_2O). Here we use the 12 day ASIS data set which includes surface waves and other supporting parameters.

The procedure for calculating fluxes is:

- w, u, v, θ, and x along with surface elevation η and, if necessary, platform motion are sampled at 10–20 Hz;
- pressure, relative humidity, sea surface temperature, and surface currents are sampled at $\sim$ 1 Hz;
- signals are quality controlled, broken into $\sim$ 20 min blocks and detrended;
- if necessary, corrections are made to account for instrument response and offset in position (see Katsaros *et al.* [51]);
- on nonstationary platforms, w, u, v, and η are corrected to account for platform motion (Anctil *et al.* [24], Drennan *et al.* [56]);
- wind vector is rotated into mean wind direction ($\bar{v} = 0$); tilt correction ($\bar{w} = 0$);
- fluxes are calculated from eqn (1); eqn (2) for H_2O and CO_2 fluxes;
- Obukhov length is calculated from eqn (5) using measured u_*, and measured (if available) or bulk heat fluxes;

- neutral 10 m mean values (U, Θ, X) are calculated using Donelan [8] profile relations;
- bulk coefficients are calculated; U_0 is neglected except in strong current environments; q_0 is calculated assuming saturated air at Θ_0, with a 2% correction for salinity effects when applicable.

Sea state parameters are also calculated. The one-dimensional parameters include: significant wave height H_s (four times the standard deviation of η), peak frequency f_p, peak phase speed c_p, and peak wavelength L_p, with the latter three being related through the dispersion relationship. In addition, directional wave spectra are calculated using data from multiple wave sensors. Here we use arrays of surface elevation gauges; wave buoys provide similar data—see Pettersson *et al.* [57]. Finally, a wave-partitioning algorithm (e.g. Gerling [58]) is used to separate the wave field into its components. For each wave train, the energy, peak frequency, and peak propagation direction are calculated.

The sea state is classified based on the wind and wave parameters. At most one wave component is designated wind sea, the most energetic component meeting the following criteria: (i) $U_{10N} \cos(\theta_d)/c_p > 0.83$, where θ_d is the angle between the mean wind and waves (Donelan *et al.* [59]), and (ii) $|\theta_d| < 45°$. Any other wave components are classified as swell. A sea is termed wind sea dominant (WSD) if the energy of the wind sea E(ws) exceeds that of the swell(s), E(swell). If E(ws) $> 5E$(swell), the sea is denoted pure wind sea (PWS). Similar definitions are used for swell-dominated and pure swell conditions.

Figure 1 shows a plot of a compilation of eddy correlation momentum flux data (2464 points) from the eight field experiments. The Smith [60] bulk relation,

$$C_{DN} = (0.61 + 0.063 U_{10N}) \times 10^{-3}, \tag{13}$$

shown in Fig. 1, is typical of many drag coefficient curves. The Smith curve is seen to agree reasonably well with the mean of the data at most wind speeds. The drag coefficient as calculated assuming a constant Charnock parameter of 0.015, the mean for these data in the range $5 \leq U \leq 16$ m/s, provides a slightly improved agreement. However, it is clear that: (i) at moderate to high winds there are a considerable number of points which are much larger than predicted; (ii) at low winds the data are systematically larger than predicted. We discuss each of these points below.

5 Momentum flux

5.1 Light winds: gustiness and smooth flow

From Fig. 1 it is evident that the highest degree of scatter occurs at low winds. There are several reasons for this. In the free convection limit, as $U \to 0$, shear becomes unimportant, and the friction velocity is no longer a useful scaling variable. It is, however, frequently observed that low wind speeds are often associated

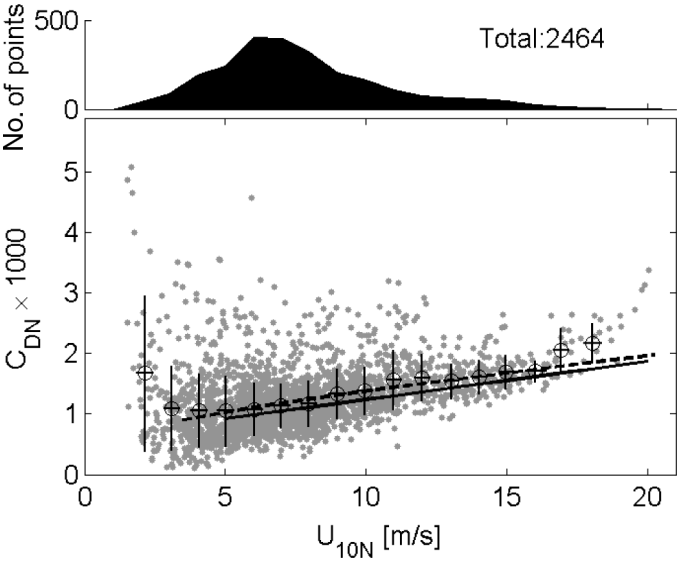

Figure 1: 10 m neutral drag coefficient versus 10 m neutral wind speed for eight field experiments. Also shown are the bulk relation of Smith [60] (solid line) and the drag relation calculated with a constant Charnock parameter of 0.015 (dashed line). The circles represent data averaged in wind speed bins of 1 m/s, showing 1 standard deviation in U_{10N} and C_{DN}. The wind speed distribution of the data is shown in the top panel.

with high variability in both speed and direction. This gustiness is associated with large-scale coherent structures in the convective boundary layer (CBL). Businger [61] introduced a new velocity scale, the convective velocity scale, $w_* = (F_B\, z_i)^{1/3}$ to account for the intermittent effects of gustiness. Here z_i is the CBL height. In light wind conditions, Godfrey and Beljaars [62] proposed replacing the mean wind speed with an effective wind speed (U_E), taking into account the gustiness: $U_E^2 = U^2 + u_g^2$, where $u_g = \beta w_*$, and $\beta \approx 1.25$ is a constant. According to Grachev and Fairall [63], gustiness is expected to lead to significant departures from the MO theory for $u_g/U > 0.5$, and must be taken into account in these conditions. During the TOGA-COARE experiment, when winds were below 4 m/s roughly half the time, the convective threshold was met 7.5% of the time (Grachev and Fairall [63]).

The Charnock roughness parameterization assumes the surface roughness to be due entirely to the presence of small-scale gravity waves. This is known as the "rough flow" regime (roughness Reynolds number, $Re_* = u_* z_0/\nu > 2.2$), and is valid for most wind speeds. However at low winds, the viscosity ν also plays a role in supporting the surface stress. In smooth flow conditions ($Re_* < 0.13$), the roughness length is given by $z_0 = 0.11 u_*/\nu$ (Kraus and Businger [41]). For intermediate Reynolds numbers, Smith [64] proposed the roughness to be the sum

of Charnock and smooth flow values:

$$z_0 = 0.11u_*/v + \alpha u_*^2/g. \tag{14}$$

Many current bulk algorithms, such as Fairall *et al.* [65, 66] and Zeng *et al.* [67], use eqn (14) for momentum roughness length. These algorithms, as well as Bourassa *et al.* [68], also take into account the effects of gustiness.

Smooth flow effects become significant for wind speeds under about 4 m/s, and lead to an increasing roughness with decreasing wind for $U < 3$ m/s. Although this is qualitatively consistent with the data in Fig. 1, the smooth flow effect is not sufficient to account for the large observed increase in drag at low winds. At $U = 0.5$ m/s, the smooth flow drag coefficient is expected to be 0.0012, significantly lower than the observed range of 0.002–0.005.

Bourassa *et al.* [68] attempted to account for this discrepancy by including the effects of capillary waves. Following Wu [69], the roughness length for capillary waves is given by $z_{0c} = 0.18\sigma/(u_*^2\rho_w)$, where σ is the surface tension and ρ_w is the density of water. Including this term in the roughness length leads to a strong increase in C_{DN} as U decreases below 4 m/s, with $C_{DN} \approx 0.002$ for $U \approx 1$ m/s. This is discussed further below.

5.2 The effect of sea state: wave age and steepness

Offshore flows near the coast are typically associated with significantly higher drag coefficients than are predicted by eqn (13). This is demonstrated in Fig. 2a, where the WAVES data from the near-shore of Lake Ontario (Drennan *et al.* [45]) are seen to be significantly above eqn (13) on average. In Fig. 2b, all wind sea data from the combined data set are plotted and divided into two groups based on inverse wave age, u_*/c_p. It is evident that the younger waves ($u_*/c_p \geq 0.1$, black points) are associated with a higher drag coefficient. This is the so-called wave-age, or fetch, effect.

As shown definitively in the JONSWAP experiment (Hasselmann *et al.* [70]; Komen *et al.* [71]), the wave energy and period increase with fetch $\tilde{X}$ reaching their asymptotic "fully-developed" values for dimensionless fetches ($\tilde{X}g/u_*^2$) of order 10^7. The dispersive nature of surface waves implies that they propagate more rapidly with increasing wavelength or period. For typical values of wind speed, full development occurs at $\tilde{X} = O(1000\,\text{km})$.

Kitaigorodskii and Volkov [72] included the wave age in their expression for z_0, taking into account the speed of the roughness elements relative to the wind. This can be incorporated into the Charnock expression for roughness by assuming the Charnock parameter α to be a function of c_p/u_*. This yields an expected drag coefficient relationship of the form $C_{DN} = f(U_{10N}, c_p/u_*)$. Experimental support for this was first presented by Donelan [73]. Subsequent attempts to quantify the relationship were often hampered by several effects. In particular, for many data sets self-correlation between the dimensionless roughness (z_0/H_s) and the wave age (c_p/u_*) has been a problem. Here the self-correlation arises because z_0 is calculated

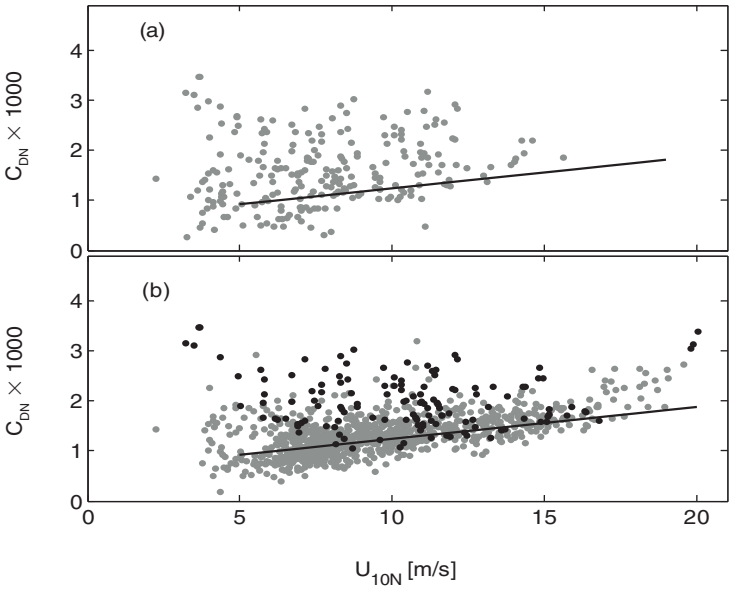

Figure 2: (a) Drag coefficient at 10 m, $C_{\mathrm{DN}} = (u_*/U_{10})^2$ versus 10 m neutral wind speed, $U_{10\mathrm{N}}$, for the WAVES experiment. (b) C_{DN} versus $U_{10\mathrm{N}}$ for WSD data (eight experiments). Points with $u_*/c_{\mathrm{p}} \geq 0.1$ are black. The Smith [60] bulk relation is shown in both panels.

via eqn (7a) from the friction velocity, and hence both the roughness and the wave age depend on u_*.

Recently, Drennan *et al.* [53] using five carefully selected PWS data sets, and an approach designed to minimize spurious correlations, found

$$z_0/H_{\mathrm{s}} = 3.35(c_{\mathrm{p}}/u_*)^{-3.4} \tag{15}$$

or equivalently

$$z_0 g/u_*^2 = 1.7(c_{\mathrm{p}}/u_*)^{-1.7}. \tag{16}$$

Either expression for roughness implies that fetch-limited waves are significantly rougher than their open ocean counterparts (except in duration limited events), and that the fetch-limited momentum transfer (through C_{DN}) is significantly higher. For instance, drag coefficients for young waves with $c_{\mathrm{p}}/u_* = 10$ are 30–50% higher (depending on wind speed) than predicted by eqn (13).

Although these results were derived for PWS data, they are also valid for the less restrictive case of WSD data. In Fig. 3, we plot the dimensionless roughness versus inverse wave age for the combined WSD data. The PWS subset of these data (659 of the 1069 points) is denoted with dots. There is no significant difference between the two sets; eqn (15) is valid for all WSD data, not just PWS. Conversely, eqn (15) is

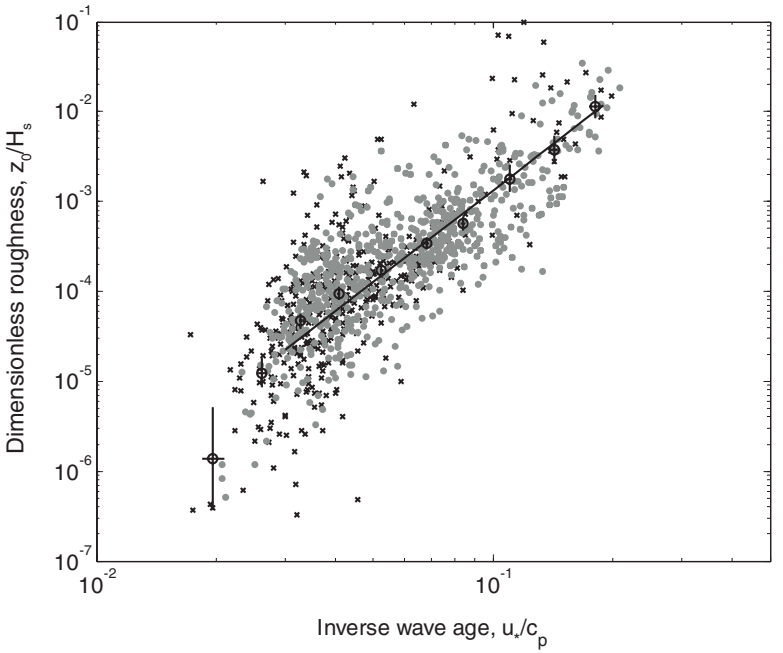

Figure 3: Dimensionless roughness versus inverse wave age for the combined WSD data set. Grey dots denote the PWS subset. The circles show means of data binned into 10 wave-age groups, with 2 standard errors indicated. The line is from Drennan *et al.* [53].

not valid in swell-dominated situations. This is seen in Fig. 4, where the roughness z_0/H_s from the 1395 swell-dominated cases are plotted.

The wave-age effect is strongest within $O(10\,\text{km})$ from the coast, but in stronger winds extends to $O(100\,\text{km})$. During the recent FETCH experiment in the Mediterranean, offshore high wind Mistral flows ($U \sim 16\,\text{m/s}$) produced significantly enhanced stress at the ASIS buoy 50 km offshore (Drennan *et al.* [53]).

Taylor and Yelland [74] have presented an alternative scaling to account for sea state effects. In terms of the wave steepness H_s/L_p they find

$$z_0/H_s = 1200(H_s/L_p)^{4.5}, \tag{17}$$

where L_p is the peak wavelength. The wave steepness relation was found to be well supported by a variety of data sets, including open ocean mixed-sea conditions, but not strongly forced near-shore (fetch-limited) data.

Drennan *et al.* [75] recently compared, and evaluated, the two sea state formulations. Their conclusions are: (i) in WSD conditions, both eqns (15) and (17) yield significant improvements over standard bulk algorithms; (ii) the wave-age scaling yields the best results in fetch-limited (strongly forced) conditions; (iii) for general

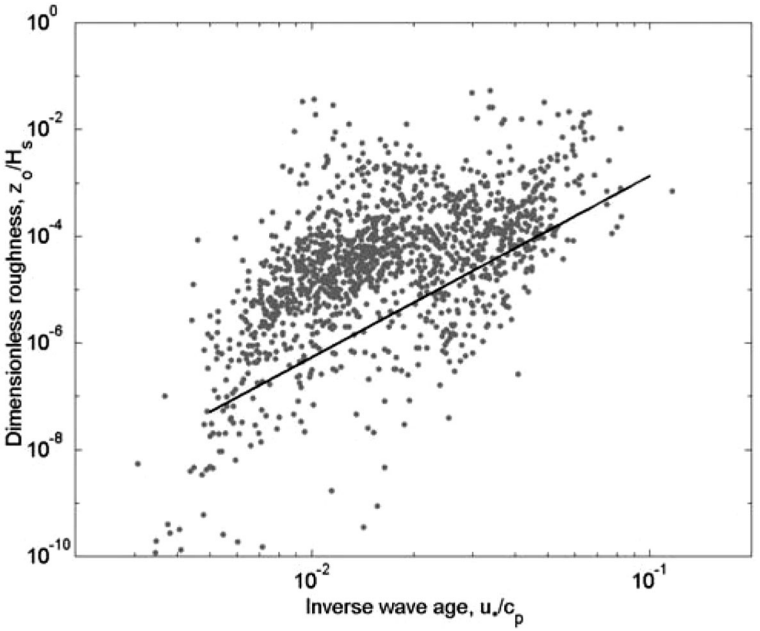

Figure 4: Dimensionless roughness versus inverse wave age for swell-dominated data. The wave-age formula (—) of Drennan *et al.* [53], developed for wind sea conditions, is seen to underpredict most swell data.

mixed seas, the wave steepness is preferred over both wave age and bulk scalings; (iv) in swell-dominated conditions, standard bulk algorithms provide better stress estimates than either sea state scaling.

The application of a sea state formulation requires information (preferably directional) on the wave field. Although many older data sets do not include such parameters, many modern ones do—either from direct or satellite measurements, or via wave models (e.g. Komen *et al.* [71]). To date, few bulk algorithms take sea state effects into account. Exceptions are Bourassa *et al.* [68], Clayson *et al.* [76], and Fairall *et al.* [66]. The first two combine the Smith *et al.* [47] wave-age formulation $z_0 g/u_*^2 = 0.48(c_\mathrm{p}/u_*)^{-1}$, similar to eqn (16), with a capillary wave term for low winds. Fairall *et al.* [66] include both wave-age and wave steepness effects as optional inputs.

We emphasize here that the use of a sea state parameterization as part of a general bulk formulation should only be carried out in the appropriate sea state conditions. Wave-age formulations require wind sea parameters, hence are best suited for WSD conditions. At a minimum, the Pierson–Moskowitz criterion $U_{10}/c_\mathrm{p} > 0.83$ should be met. For the wave steepness formulation Drennan *et al.* [75] propose a threshold steepness ($H_\mathrm{s}/L_\mathrm{p} > 0.02$); for lower steepness (most swell-dominated conditions) a simple wind speed dependent C_DN yields better predictions than either sea state formulation.

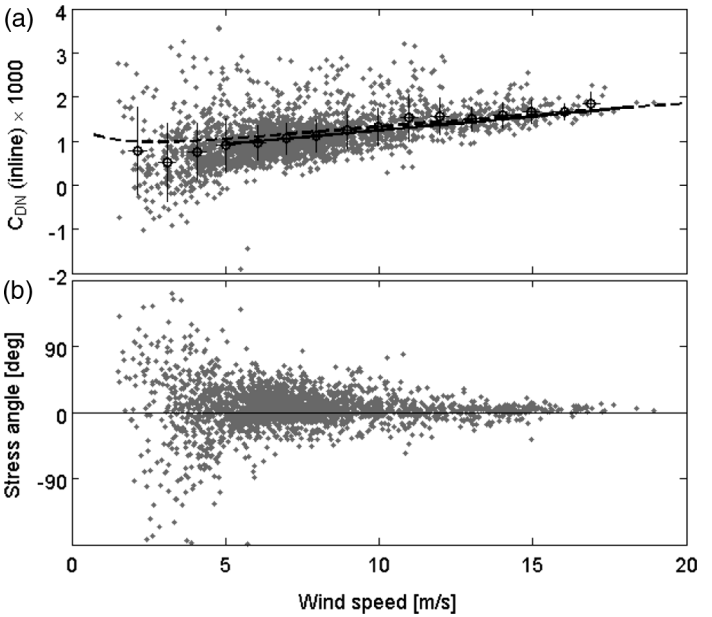

Figure 5: (a) Component of drag coefficient inline with the mean wind, $C_{DX} = -\overline{w'u'}/(U_{10N} - U_0)^2$, versus wind speed U_{10N}. The circles represent data averaged in wind speed bins of 1 m/s, showing 1 standard deviation in U and C_{DX}. The curves are for C_{DN} via Smith [60] (solid line) and Smith [64], with $z_0 = 0.11\,u_*/v + 0.012u_*^2/g$ (dashed line). (b) Stress angle with respect to the mean wind, $a\tan(\overline{w'v'}/\overline{w'u'})$, versus U_{10N}.

5.3 Sea state effects: swell

The effect of both gustiness and smooth flow would serve to increase the drag coefficient at low winds. Capillary waves have the same effect, assuming they travel in the direction of the mean wind. However, the early measurements of Volkov [16] and Makova [17] indicated significant periods of low wind where the momentum flux was lower than expected. On occasions, momentum flux was even observed to be negative (upward). These periods coincided with the presence of significant swell waves, and led the authors to speculate on a possible influence of swell on the momentum flux. Typical presentations of the drag coefficient, including Fig. 1, hide this effect as they show the magnitude of C_{DN}, which is by definition positive. Instead, in Fig. 5 we plot the component of the drag coefficient inline with the mean wind; i.e. $C_{DX} = -\overline{w'u'}/(U_{10N} - U_0)^2$. This plot excludes data from the RASEX and HEXOS experiments where only the stress magnitude is available.

It is evident that many of the low wind/high drag values in Fig. 1 have disappeared, with the data now evenly distributed about the [extended] Smith curve, even at low winds. The dashed line shows C_{DN} based on the Smith [64] roughness (14)

which includes a smooth flow correction. The Charnock parameter of 0.012, again calculated from the mean of the data, is lower than that determined earlier due to the use of a single component of stress here, instead of the magnitude. For a similar reason, the agreement with the Smith [60] curve has improved: Smith's drag coefficient was calculated from the component of stress inline with the mean wind. We note here that both definitions for C_{DN} are commonly used in the literature. The inertial dissipation method provides a third estimate, one based on the magnitude of the inline stress component.

Contrary to the situation on land (and the assumptions of the MO theory), the angle of the near-surface stress over the sea does not necessarily coincide with the angle of the wind (Fig. 5b). This was reported by Geernaert [77] who attributed it to stratification effects. Subsequent studies by Geernaert *et al.* [78] and Rieder *et al.* [79] indicate that turning is due to the effect of long waves (swells) on the short waves which form the dominant roughness scales. Grachev *et al.* [80] separated the total stress into components associated with (and traveling in the direction of) the wind waves and swell waves. The total stress was found to be oriented between the wind waves and swell. In some cases when the swell traveled in the same direction as (and faster than) the wind, the total stress was against the wind. In these cases $C_{DX} < 0$, corresponding to upward momentum flux. This phenomenon, seen in the following swell data of Fig. 6, was first noted by Volkov [16] and Makova [17]. The opposite situation with counter-swell (i.e. swell running against the wind) is seen, in Fig. 6, to yield enhanced drag coefficients (Donelan *et al.* [37]). In most following- and counter-swell cases in Fig. 6, the swells are dominant with $E(\mathrm{ws}) \ll E(\mathrm{swell})$.

Over the sea, the momentum flux is given by $\tau = \tau_{\mathrm{t}} + \tau_{\mathrm{w}} + \tau_{\mathrm{v}}$, which are the turbulent, wave-coherent, and viscous stresses, respectively. The viscous stress is significant only in a layer of $O(1\,\mathrm{mm})$ above the surface, and is neglected here. The wave-coherent stress τ_{w} accounts for the transfer of momentum to the waves. Away from the surface $\tau_{\mathrm{w}} \approx 0$, and the turbulent stress dominates the total stress. This is the classical case of boundary layer flows over land. However, as the surface is approached, there is a region where τ_{w} is significant, the so-called "wave boundary layer" (WBL). Since the total stress τ is constant, the turbulent stress (1a) is consequently reduced in the WBL. This results in the neutral wind speed profiles deviating from their expected logarithmic forms (Stewart [81]). As a result, the MO similarity theory does not apply in the WBL.

The turbulence models of Janssen [82] and Makin and Mastenbroek [83] have predicted the height of the WBL to be of the order of 1 m for PWS conditions. This would imply that the MO theory holds at typical measurement heights of $O(10\,\mathrm{m})$ in PWSs, and, indeed, recent experimental evidence (Edson and Fairall [84]; Drennan *et al.* [45]) supports this. In particular, Drennan *et al.* [45] showed that PWS spectra and cospectra representing a wide variety of wind speeds and wave ages ($U_{10\mathrm{N}} = 3.5$–$15\,\mathrm{m/s}$; $U_{10\mathrm{N}}/c_{\mathrm{p}} = 1$–$5$), and heights as low as 2 m above the surface, follow the universal curves of Miyake *et al.* [14]. Hence PWS data are expected to follow the MO theory, except perhaps very close to the surface.

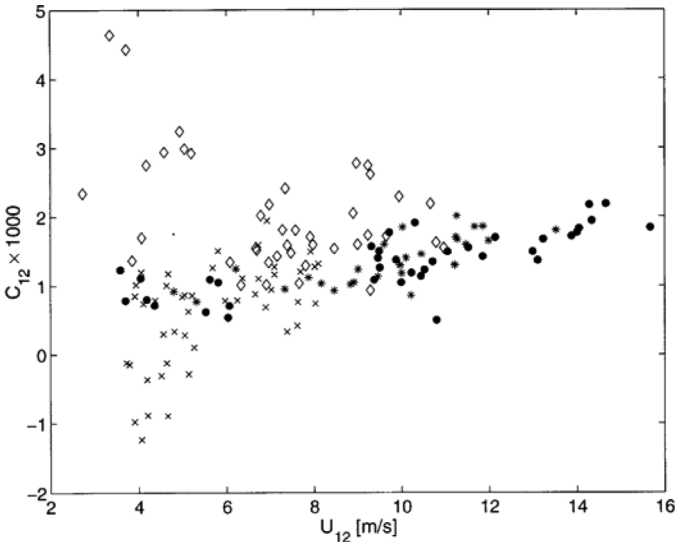

Figure 6: 12 m drag coefficients versus wind speed, showing effect of swell. Data are: PWS (●) and following swell (×) from the WAVES tower in Lake Ontario (Drennan *et al.* [45]), and PWS (∗) and counter swell (◇) from a small ship in the North Atlantic during SWADE (Donelan *et al.* [37]). The two PWS data sets, near full development, are in good agreement. The counter swell data show significantly enhanced drag; the following-swell data significantly reduced drag or even upward momentum transfer. [Reprinted from Drennan *et al.* [45] with kind permission of Kluwer Academic Publishers.]

On the other hand, in the presence of swells the WBL may extend well beyond typical measurement heights. Smedman *et al.* [85, 86] demonstrated that both the wind profiles and the TKE budget are modified when swells are present. Holland *et al.* [18] reported measurements of Donelan showing a reversal of the near-surface logarithmic wind profile ("wave-driven wind") during swells. Drennan *et al.* [45] showed that the universal spectral scaling predicted by the MO theory does not apply in swell-dominated conditions; in contrast, the spectra were supported by the wind sea data. They showed that velocity spectra (Fig. 7) and cospectra with weak–moderate winds and strong swell do not satisfy universal scaling—or MO theory—at typical measurement heights. These findings show that the wave field can significantly modify turbulence characteristics in the marine atmospheric boundary layer, and may explain some of the wide scatter observed in existing drag coefficient relationships.

To date, studies on the effects of swell on momentum flux have been largely qualitative. It is hoped that several recent experiments, along with modeling efforts (e.g. Kudryavtsev and Makin [87]), will yield considerable progress in this field in the next few years.

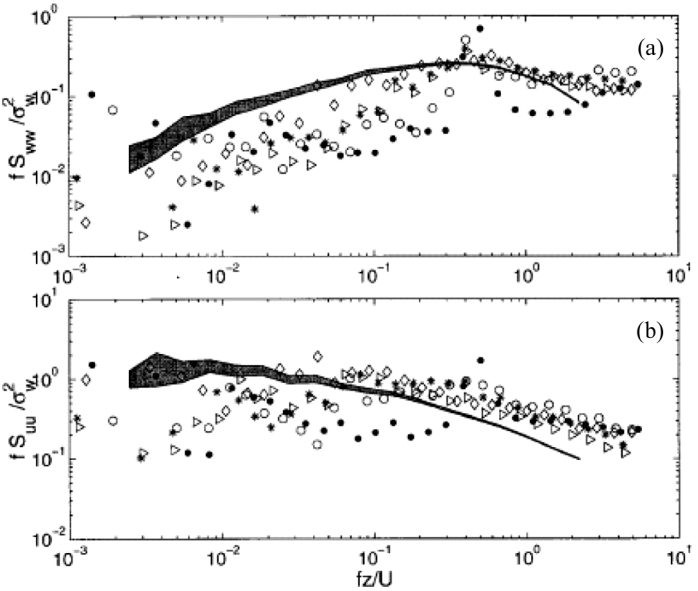

Figure 7: Spectra of vertical (a) and horizontal inline (b) velocity from five runs with strong swell, plotted in the universal scaling of Miyake *et al.* [14]. The data are in the range $U \approx 4$–5 m/s. For the $\diamond$ data, $U/c_p = 0.61$; for the other data, $U/c_p < 0.5$. The shaded areas represent ± 1 standard error about universal curves established from PWS data. [Reprinted from Drennan *et al.* [45] with kind permission of Kluwer Academic Publishers].

6 Scalar fluxes

Compared with momentum fluxes, there are relatively few scalar flux data. Although suitable anemometers have been available for decades, reliable fast-response hygrometers have been marketed only for a few years. Fast-response temperature measurements are also limited over the sea due to problems with sea spray and salt accretion on the sensors. An alternate measure of fast-response temperature can be obtained via sonic anemometry. Sonic temperature t_s, obtained from the sonic speed of sound (after corrections for cross-flow effects—see Kaimal and Gaynor [88]) is a combination of air temperature and mixing ratio: $t_s = \theta(1+0.52r)$. Hence a sonic anemometer paired with a fast-response hygrometer (or refractometer—see Delahaye *et al.* [89]) will yield the flux of sensible heat, as well as those of humidity and momentum. If a hygrometer is not available, t_s is often used as a surrogate for virtual temperature $t_v = \theta(1+0.61r)$ in calculating the buoyancy flux F_B. Sjöblom and Smedman [90] show that the mean error is this approximation is $O(1\%)$.

The HEXOS campaign of 1984–1986 provided what remains the most comprehensive set of sensible and latent heat flux data. The resulting Stanton and Dalton numbers show considerable scatter, but no significant dependence on wind speed

for winds in the range 5–20 m/s (DeCosmo *et al.* [48]). Their constant bulk values of $1.1 \times 10^{-3}(\pm 30\%)$ for both C_{HN} and C_{EN} are in the range of values $1 - 1.2 \times 10^{-3}$ given by most other studies (e.g. Large and Pond [31]).

The very different behavior of the scalar and momentum fluxes with wind speed follows from the different physical transfer mechanisms. Form drag over the roughness elements plays an important role in momentum transfer at the air–sea interface, but not in the transfer of scalar quantities. Instead, these latter transfers are controlled by diffusive processes. The well known LKB surface renewal model of Liu, Katsaros, and Businger [91] accounts for these effects, yielding roughness lengths which are functions of the roughness Reynolds number: $z_{0x}u_*/\nu = A_x Re_*^{B_x}$, where x is either q or θ and A_x and B_x vary with Re_*. The resulting expressions predict Stanton and Dalton numbers which decrease somewhat with increasing wind speed. This decrease at high winds is attributed to an increase in sheltering behind roughness elements, which increases the local turbulent renewal times, thereby reducing the transfer rates. The LKB model has been modified for use in some bulk algorithms (COARE-2.5, Fairall *et al.* [65]).

An alternative parameterization for the scalar roughness lengths, that of Brutsaert [92], is also based on surface renewal theory, with the additional assumption that the surface renewal time scale is the same as the Kolmogorov time scale for small eddies (Garratt [3]). The resulting humidity and temperature roughness lengths are $z_{0q} = z_0 \exp(2 - 2.28 Re_*^{1/4})$ and $z_{0t} = z_0 \exp(2 - 2.48 Re_*^{1/4})$, where the coefficients are those of Garratt [3]. The resulting bulk coefficients either tend to a constant value or increase somewhat (Zeng *et al.* [67]) with wind speed. This parameterization has been adopted by several current bulk algorithms, including Zeng *et al.* [67] with $z_{0q} = z_{0t} = z_0 \exp(2.57 - 2.67 Re_*^{1/4})$, and also in a modified form by COARE-3 (Fairall *et al.* [66]).

Figure 8 presents the heat flux data from several of the recent field experiments discussed above. In SWADE, temperature and humidity fluctuations were measured with a fine wire thermocouple and a Lyman-alpha humidiometer, respectively, both housed in a spray flinger (Katsaros *et al.* [51]). During the AGILE campaign, a fine wire dry thermistor and wicked wet-bulb thermistor were used to measure temperature and humidity (Donelan and Drennan [93]). Humidity fluctuations were measured during GASEX-2001 with a LICOR-7500 open path humidiometer.

The Stanton numbers from SWADE and AGILE for $|\Delta\Theta| = |\Theta_z - \Theta_0| > 2°C$ are plotted in Fig. 8a. The threshold is applied taking into account that the measured "surface" Θ_0 is rarely the true skin temperature but instead a bulk temperature at several meters depth. Since the bulk and skin temperatures can differ by $O(1°C)$—see Fairall *et al.* [94]—the threshold reduces the error in $\Delta\Theta$, with the value of 2°C chosen so as to reduce the scatter.

The C_{HN} data show considerable variability, but no significant wind speed dependence. There is, however, a significant difference between the Stanton numbers for stable and unstable stratification, with the stable data exhibiting considerably lower C_{HN} values. This was observed by Large and Pond [31], and Oost *et al.* [95].

Dalton numbers from SWADE, AGILE, and GASEX are plotted in Fig. 8b. Although there is considerable scatter, the three data sets are in agreement, with

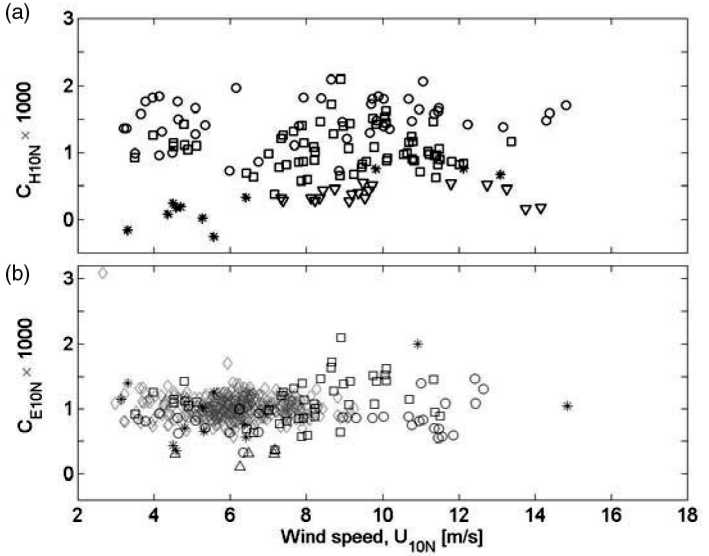

Figure 8: (a) Stanton numbers from two field experiments. SWADE (Katsaros *et al.* [51]): □ (unstable), ∇ (stable); AGILE (Donelan and Drennan [93]): ○ (unstable), ∗ (stable). (b) Dalton numbers from three field campaigns: □, ○, ∗ (as above); AGILE: Δ (condensing); GASEX: ◇ (unstable).

a mean $C_{EN} = 1.02 \pm 0.2 \times 10^{-3}$. The data do not exhibit significant wind speed dependence, nor is there a dependence on stability. However, the few points taken in condensing flows (downward humidity transport) exhibit a significantly lower bulk coefficient.

For several decades, it has been predicted that the presence of sea spray should lead to increased evaporation rates at high winds (e.g. Andreas *et al.* [96]). This claim, which has been the source of several vigorous debates (summarized in Andreas and DeCosmo [97]), remains to be supported by experimental data. Although DeCosmo *et al.* [48] did not find a significant wind speed dependence in the HEXOS C_{EN} values, Andreas and DeCosmo [97] claim a spray enhancement of 10–40% in the same data for $U \sim 15$–18 m/s. However, this enhancement is compared with the values predicted by an LKB-type model which, as pointed out above, decrease at high winds. The net effect is the observed constant Dalton number.

The large scatter in typical Dalton and Stanton number plots (e.g. Fig. 8) continues to hinder efforts to parameterize the bulk coefficients. The data do not allow one to distinguish between simple constant bulk coefficients and theoretical predictions where the roughness is a function of Re_*. Likewise, the data alone do not show an enhancement of humidity flux due to sea spray.

Finally, we briefly summarize current progress on CO_2 flux parameterization, referring the reader to Fairall *et al.* [5] for further details. As reliable fast-response

CO_2 sensors have only been available for a few years, micrometeorological estimates of CO_2 flux are relatively rare (McGillis *et al.* [38, 55]; Donelan and Drennan [50]; Jacobs *et al.* [98]). Although these new results have considerable scatter, they agree fairly well with the earlier chemical tracer estimates of Wanninkhof [99] and Watson *et al.* [100]. Nevertheless, there remains considerable uncertainty on the wind speed dependence of the CO_2 bulk transfer coefficient, especially at high winds, and on what other factors control the air–sea flux. This remains a subject of active research.

7 Discussion

We have summarized the current state of air–sea flux parameterizations and, in particular, how they depend on sea state. Two separate sea state effects were discussed. The "wave-age" effect relates to the increased roughness (momentum transfer) over young, fetch- or duration-limited, waves compared with fully developed ones. Wave age has been included in some recent bulk parameterizations, although additional steps must be taken to ensure that the algorithm is only applied when wind sea parameters are available (from 2D wave spectra, or in WSD conditions).

The swell effect, which remains qualitative at this point, can be significant at low–moderate winds, when strong swells are present. Swell waves can either increase or decrease the drag, depending on the relative direction and amplitude of the swell compared with the wind sea. Bourassa *et al.* [68] attempted to include swell effects in their bulk algorithm by including wave direction in a wave-age term. However, wave-age expressions are developed for wind sea conditions and are not applicable to swell. The inclusion of swell effects in bulk parameterizations awaits a better understanding of how swell influences the air–sea transfers.

Regarding the fluxes of humidity and sensible heat, experimental evidence to date supports constant bulk coefficients, independent of wind speed. The scatter in the data is sufficient that a slight increase (or decrease) in C_{EN} with wind speed cannot be ruled out, but it is not significant. As yet, there is no support for a spray-induced enhancement of C_{EN} above the constant value.

One limitation of all bulk parameterizations is their application in high wind conditions. To date, very few data have been collected at wind speeds above 20 m/s. Hence, the algorithms remain unvalidated in this regime. Although it is common practice to simply extrapolate the present curves to higher winds, this approach is questionable, as characteristics of the sea surface change with increasing wind.

As the wind speed increases the waves become steeper and breaking is more widespread—see for instance Fig. 9, a photograph of the sea surface taken from 470 m during Hurricane Isabel. The laboratory study of Reul *et al.* [101] demonstrates that flow separation increases significantly behind steep breaking waves. Large quantities of spray are also produced, which may effect heat and humidity transfer (as discussed above), and perhaps momentum transfer if the spray density becomes sufficiently high. As the production of both spray and bubbles increases the surface itself is no longer well defined, potentially affecting all transfer processes.

Figure 9: Sea surface between rain bands of category 5 Hurricane Isabel. Photo taken by the author from NOAA–AOC aircraft N43RF on September 14, 2003 during the CBLAST experiment. The altitude is 470 m and the flight level wind speed is 50 m/s.

One topic of considerable recent interest concerns hurricanes. The ongoing ONR-sponsored Coupled Boundary Layer/Air–Sea Transfer (CBLAST) hurricane experiment has a primary focus on increasing our understanding of tropical storm dynamics, and on improving hurricane model accuracy. Hurricanes present a problem for today's bulk parameterizations. Bulk parameterizations predict drag coefficients as increasing roughly linearly with wind speed, but constant Dalton and Stanton numbers. For instance, using the results of Smith [60] at 35 m/s, $C_D \approx 0.003$ and $C_E \approx 0.0012$. The wave-age formulation (15), using wave spectral data from a scanning radar altimeter (SRA) in Hurricane Bonnie, Wright *et al.* [102], predicts drag coefficients roughly 50% higher than Smith [60]—see Fig. 10. Here the predictions for Hurricane Bonnie are estimated only for wave spectra exhibiting a distinct wind sea component.

However, Emanuel [104] has shown that typical hurricane models cannot develop a model storm under the extrapolated predictions of present bulk formulae. Model hurricanes develop only when momentum and enthalpy exchange coefficients are roughly equal. Either the enthalpy flux (a combination of sensible and latent heat fluxes) must increase at higher winds or the drag coefficient must decrease. Powell *et al.* [105] have presented data in support of the latter: their estimates of u_*, based on vertical profiles of wind speed from GPS dropsondes, level off when wind speeds reach hurricane levels; even at wind speeds below 30 m/s their drag values are significantly below the Smith [60] predictions. At the same time, Andreas and Emanuel [106] have shown that spray can significantly increase the enthalpy flux if it reenters the sea before completely evaporating.

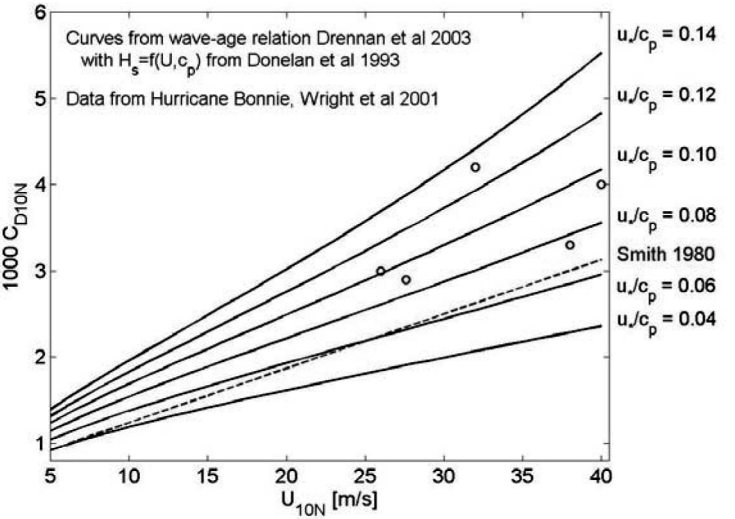

Figure 10: Estimated drag coefficient versus wind speed during Hurricane Bonnie. The estimates are made using SRA wave spectra from Wright *et al.* [102], along with the wave-age relations of Drennan *et al.* [53]. The curves are from [53], with the H_S relation of Donelan *et al.* [103].

Clearly there is a need for measurements of momentum, heat, and humidity fluxes, along with sea state and sea spray, in the high-wind regime. This is one of the goals of CBLAST, and the 2003 campaign has yielded a promising data set. The results should allow for improved flux parameterization at high winds, and ultimately improved coupled ocean–atmosphere models.

Acknowledgments

Financial support from the US National Science Foundation (grant OCE-9871855) and the US Office of Naval Research (grants N00014-00-1-0594 and N00014-01-F-009) is gratefully acknowledged. Thanks also to Dr. Will Perrie for his helpful comments and suggestions, and to Patricia Archuleta and Maria Calderin for assistance with the typesetting.

References

[1] Shindell, D.T., Miller, R.L., Schmidt, G.A. & Pandolfo, L., Simulation of recent northern winter climate trends by greenhouse-gas forcing. *Nature*, **399**, pp. 452–455, 1999.

[2] Bao, J.-W., Wilczak, J.M., Choi, J.-K. & Kantha, L.H., Numerical simulations of air–sea interaction under high wind conditions using a coupled

model: a study of hurricane development. *Monthly Weather Review*, **128**, pp. 2190–2210, 2000.

[3] Garratt, J.R., *The Atmospheric Boundary Layer*, Cambridge University Press: Cambridge and New York, 1992.

[4] Webb, E.K., Pearman, G.I. & Leuning, R., Correction of flux measurements for density effects due to heat and water vapour transfer. *Quarterly Journal of the Royal Meteorological Society*, **106**, pp. 85–100, 1980.

[5] Fairall, C.W., Hare, J.E., Edson, J.B. & McGillis, W., Parameterization and micrometeorological measurement of air-sea gas transfer. *Boundary-Layer Meteorology*, **96**, pp. 63–105, 2000.

[6] Monin, A.S. & Obukhov, A.M., Basic laws of turbulent mixing in the ground layer of the atmosphere. *Akad. Nauk. SSSR Geofiz. Inst. Tr.*, **151**, pp. 163–187, 1954.

[7] Busch, N.E., On the mechanics of atmospheric turbulence (Chapter 1). *Workshop on Micro-meteorology*, ed. D.A. Haugen, American Meteorological Society: Boston, pp. 1–65, 1973.

[8] Donelan, M.A., Air–sea interaction. *The Sea: Ocean Engineering Science*, 9, eds B. LeMéhauté D. Hanes, John Wiley and Sons, Inc.: New York, pp. 239–292, 1990.

[9] Högström, U., Nondimensional wind and temperature profiles in the atmospheric surface layer: a re-evaluation. *Boundary-Layer Meteorology*, **42**, pp. 55–78, 1988.

[10] Zilitinkevich, S.S. & Chalikov, D.V., Determining the universal wind velocity and temperature profiles in the atmospheric boundary layer. *Izvestiya, Atmospheric and Oceanic Physics*, **4**, pp. 165–170, 1968.

[11] Dyer, A.J. & Hicks, B.B., Flux-gradient relationships in the constant flux layer. *Quarterly Journal of the Royal Meteorological Society*, **96**, pp. 715–721, 1970.

[12] Businger, J.A., Wyngaard, J.C., Izumi, Y.K. & Bradley, E.F., Flux-profile relationships in the atmosphere surface layer. *Journal of the Atmospheric Sciences*, **28**, pp. 181–189, 1971.

[13] Högström, U., Review of some basic characteristics of the atmospheric surface layer. *Boundary-Layer Meteorology*, **78**, pp. 215–246, 1996.

[14] Miyake, M., Stewart, W. & Burling, R.W. Spectra and cospectra of turbulence over water. *Quarterly Journal of the Royal Meteorological Society*, **96**, pp. 138–143, 1970.

[15] Pond, S., Phelps, G.T., Paquin, J.E., McBean, G. & Stewart, R.W. Measurements of the turbulent fluxes of momentum, moisture and sensible heat over the ocean. *Journal of the Atmospheric Sciences*, **28**, pp. 901–917, 1971.

[16] Volkov, Y.A., Turbulent flux of momentum and heat in the atmospheric surface layer over a disturbed surface. *Izvestiya, Atmospheric and Oceanic Physics*, **6**, pp. 770–774, 1970.

[17] Makova, V.I., Features of the dynamics of turbulence in the marine atmospheric surface layer at various stages in the development of waves. *Izvestiya, Atmospheric and Oceanic Physics*, **11**, pp. 297–307, 1975.

[18] Holland, J.Z., Chen, W., Almazan, J.A. & Elder, F.C., Atmospheric boundary layer. *IFYGL—The International Field Year for the Great Lakes*, eds E.J. Aubert & T.L. Richards, NOAA: Ann Arbor, pp. 109–167, 1981.

[19] Paulson, C.A., Leavitt, E. & Fleagle, R.G. Air-sea transfer of momentum, heat and water determined from profile measurements during BOMEX. *Journal of Physical Oceanography*, **2**, pp. 487–497, 1972.

[20] Davidson, K.L., Observational results on the influence of stability and wind-wave coupling on momentum transfer and turbulent fluctuations over ocean waves. *Boundary-Layer Meteorology*, **6**, pp. 305–331, 1974.

[21] Kaimal, J.C., Wyngaard, J.C., Izumi, Y. & Coté, O.R., Spectral characteristics of surface-layer turbulence. *Quarterly Journal of the Royal Meteorological Society*, **98**, pp. 563–589, 1972.

[22] Mahrt, L., Vickers, D., Howell, J., Højstrup, J., Wilczak, J.M., Edson, J. & Hare, J., Sea surface drag coefficients in the Risø Air Sea Experiment. *Journal of Geophysical Research*, **101**, pp. 14327–14335, 1996.

[23] Axford, D.N., On the accuracy of wind measurements using an inertial platform in an aircraft, and an example of a measurement of the vertical mesostructure of the atmosphere. *Journal of Applied Meteorology*, **7**, pp. 645–666, 1968.

[24] Anctil, F., Donelan, M.A., Drennan, W.M. & Graber, H.C., Eddy correlation measurements of air-sea fluxes from a Discus buoy. *Journal of Atmospheric and Oceanic Technology*, **11**, pp. 1144–1150, 1994.

[25] Edson, J.B., Hinton, A.A., Prada, K.E., Hare, J.E. & Fairall, C.W., Direct covariance flux estimates from mobile platforms at sea. *Journal of Atmospheric and Oceanic Technology*, **15**, pp. 547–562, 1998.

[26] Wieringa, J., A revaluation of the Kansas mast influence on measurements of stress and cup anemometer overspeeding. *Boundary-Layer Meteorology*, **18**, pp. 411–430, 1980.

[27] Wyngaard, J.C., The effects of probe-induced flow distortion on atmospheric turbulence measurements. *Journal of Applied Meteorology*, **20**, pp. 784–794, 1981.

[28] Yelland, M.J., Moat, B.I., Taylor, P.K., Pascal, R.W., Hutchings, J. & Cornell, V.C., Wind stress measurements from the open ocean corrected for airflow distortion by the ship. *Journal of Physical Oceanography*, **28**, pp. 1511–1526, 1998.

[29] Dupuis, H., Guérin, C., Hauser, D., Weill, A., Nacass, P., Drennan, W.M., Cloché, S. & Graber, H.C., Impact of flow distortion corrections on turbulent fluxes estimated by the inertial dissipation method during the FETCH experiment on R/V L'Atalante. *Journal of Geophysical Research*, **108**(C3), 8064, doi:10.1029/2001JC001075, 2003.

[30] Pedreros, R., Dardier, G., Dupuis, H., Graber, H.C., Drennan, W.M., Weill, A., Guérin, C. & Nacass, P., Momentum and heat fluxes via the eddy correlation method on the R/V L'Atalante and an ASIS buoy. *Journal of Geophysical Research*, **108**(C11), 3339, doi:10.1029/2002JC001449, 2003.

[31] Large, W.G. & Pond, S., Sensible and latent heat flux measurements over the ocean. *Journal of Physical Oceanography*, **12**, pp. 464–482, 1982.

[32] Large, W.G. & Pond, S., Open ocean momentum flux measurements in moderate to strong winds. *Journal of Physical Oceanography*, **11**, pp. 324–336, 1981.

[33] Dupuis, H., Taylor, P.K., Weill, A. & Katsaros, K., Inertial dissipation method applied to derive turbulent fluxes over the ocean during the Surface of the Ocean, Fluxes and Interactions with the Atmosphere/Atlantic Stratocumulus Transition Experiment (SOFIA/ASTEX) and Structure des Echanges
Mer-Atmosphere, Proprietes des Heterogeneites Oceaniques: Recherche Experimentale (SEMAPHORE) experiments with low to moderate wind speeds. *Journal of Geophysical Research*, **102**, pp. 21115–21129, 1997.

[34] Sjöblom, A. & Smedman, A.S., Vertical structure in the marine atmospheric boundary layer and its implication for the inertial dissipation method. *Boundary-Layer Meteorology*, **109**, pp. 1–25, 2003.

[35] Janssen, P.A.E.M., On the effect of ocean waves on the kinetic energy balance and consequences for the inertial dissipation method. *Journal of Physical Oceanography*, **29**, pp. 530–534, 1999.

[36] Taylor, P.K. & Yelland, M.J., Comments on "On the effect of ocean waves on the kinetic energy balance and consequences for the inertial dissipation method". *Journal of Physical Oceanography*, **31**, pp. 2532–2536, 2001.

[37] Donelan, M.A., Drennan, W.M. & Katsaros, K.B., The air-sea momentum flux in conditions of mixed wind sea and swell. *Journal of Physical Oceanography*, **27**, pp. 2087–2099, 1997.

[38] McGillis, W.R., Edson, J.B., Ware, J.D., Dacey, J.W.H, Hare, J.E., Fairall, C.W. & Wanninkhof, R., Carbon dioxide flux techniques performed during GasEx-98. *Marine Chemistry*, **75**, pp. 267–280, 2001.

[39] Brunke, M.A., Fairall, C.W., Zeng, X., Eymard, L. & Curry, J.A., Which bulk aerodynamic algorithms are least problematic in computing ocean surface turbulent fluxes? *Journal of Climate*, **16**, pp. 619–635, 2003.

[40] Charnock, H., Wind stress on a water surface. *Quarterly Journal of the Royal Meteorological Society*, **81**, pp. 639–640, 1955.

[41] Kraus E.B. & Businger, J.A., *Atmosphere-Ocean Interaction.* Oxford University Press: New York, 1994.

[42] Geernaert, G.L., Bulk parameterization for the wind stress and heat fluxes. *Surface Waves and Fluxes*, eds G.L. Geernaert & W.J. Plant, Kluwer: Dordrecht, pp. 91–172, 1990.

[43] Sreenivasan, K.R., Chambers, A.J. & Antonia, R.J., Accuracy of moments of velocity and scalar fluctuations in the atmospheric surface layer. *Boundary-Layer Meteorology*, **14**, pp. 341–359, 1978.

[44] Donelan, M.A., Madsen, N., Kahma, K., Tsanis, I.K. & Drennan, W.M., Apparatus for atmospheric boundary layer measurements over waves. *Journal of Atmospheric and Oceanic Technology*, **16**, pp. 1172–1182, 1999.

[45] Drennan, W.M., Kahma, K.K. & Donelan, M.A., On momentum flux and velocity spectra over waves. *Boundary-Layer Meteorology*, **92**, pp. 489–515, 1999.

[46] Johnson, H.K., Højstrup, J., Vested, H.J. & Larsen, S.E., On the dependence of sea surface roughness on wind waves. *Journal of Physical Oceanography*, **28**, pp. 1702–1716, 1998.

[47] Smith, S.D., Anderson, R.J., Oost, W.A., Kraan, C., Maat, N., deCosmo, J., Katsaros, K.B., Davidson, K.L., Bumke, K., Hasse, L. & Chadwick, H.M., Sea surface wind stress and drag coefficients: the HEXOS results. *Boundary-Layer Meteorology*, **60**, pp. 109–142, 1992.

[48] DeCosmo, J., Katsaros, K.B., Smith, S.D., Anderson, R.J., Oost, W.A., Bumke, K. & Chadwick, H., Air-sea exchange of water and sensible heat: The Humidity Exchange Over the Sea (HEXOS) results. *Journal of Geophysical Research*, **101**, pp. 12001–12016, 1996.

[49] Janssen, J.A.M., Does wind stress depend on sea state or not? A statistical analysis of HEXMAX data. *Boundary-Layer Meteorology*, **83**, pp. 479–503, 1997.

[50] Donelan, M.A. & Drennan, W.M., Direct field measurements of the flux of carbon dioxide. *Air-Water Gas Transfer*, eds B. Jähne & E.C. Monahan, Aeon-Verlag: Hanau, pp. 677–683, 1995.

[51] Katsaros, K.B., Donelan, M.A. & Drennan, W.M., Flux measurements from a Swath ship in SWADE. *Journal of Marine Systems*, **4**, pp. 117–132, 1993.

[52] Graber, H.C., Terray, E.A., Donelan, M.A., Drennan, W.M., Van Leer, J. & Peters, D.B., ASIS—A new air-sea interaction spar buoy: design and performance at sea. *Journal of Atmospheric and Oceanic Technology*, **17**, pp. 708–720, 2000.

[53] Drennan, W.M., Graber, H.C., Hauser, D. & Quentin, C., On the wave age dependence of wind stress over pure wind seas. *Journal of Geophysical Research*, **108**(C3), 8062, doi:10.1029/2000JC000715, 2003.

[54] Dhanak, M.R., An, P.E. & Holappa, K., An AUV survey in the littoral zone: small-scale subsurface variability accompanying synoptic observations of surface currents. *IEEE Journal of Oceanic Engineering*, **26**, pp. 752–768, 2003.

[55] McGillis, W.G., Edson, J.B., Zappa, C.J., Ware, J.D., McKenna, S.P., Terray, E.A., Hare, J.E., Fairall, C.W., Drennan, W., Donelan, M., DeGrandpre, M.D., Wanninkhof, R. & Feely, R.A., Air-sea CO_2 exchange in the Equatorial Pacific. *Journal of Geophysical Research*, **109**, C08S02, doi:10.1029/2003JC002256, 2004.

[56] Drennan, W.M., Donelan, M.A., Madsen, N., Katsaros, K.B., Terray, E.A. & Flagg, C.N., Directional wave spectra from a Swath ship at sea. *Journal of Atmospheric and Oceanic Technology*, **11**, pp. 1109–1116, 1994.

[57] Pettersson, H., Graber, H.C., Hauser, D., Quentin, C., Kahma, K.K., Drennan, W.M. & Donelan, M.A., Directional wave measurements from three wave sensors during the FETCH experiment. *Journal of Geophysical Research*, **108**(C3), 8061, doi:10.1029/2001JC001164, 2003.

[58] Gerling, T.W., Partitioning sequences and arrays of directional ocean wave spectra into component wave systems. *Journal of Atmospheric and Oceanic Technology*, **9**, pp. 444–458, 1992.
[59] Donelan, M.A., Hamilton, J. & Hui, W.H., Directional spectra of wind generated waves. *Philosophical Transactions of the Royal Society of London*, **A315**, pp. 509–562, 1985.
[60] Smith, S.D., Wind stress and heat flux over the ocean in gale force winds. *Journal of Physical Oceanography*, **10**, pp. 709–726, 1980.
[61] Businger, J.A., A note on free convection. *Boundary-Layer Meteorology*, **4**, pp. 323–326, 1973.
[62] Godfrey, J.S. & Beljaars, A.C.M., On the turbulent fluxes of buoyancy, heat and moisture at the air-sea interface at low wind speeds. *Journal of Geophysical Research*, **96**, pp. 22043–22048, 1991.
[63] Grachev, A.A. & Fairall, C.W., Dependence of the Monin-Obukhov stability parameter on the bulk Richardson number over the ocean. *Journal of Applied Meteorology*, **36**, pp. 406–415, 1997.
[64] Smith, S.D., Coefficients for sea surface wind stress, heat flux and wind profiles as a function of wind speed and temperature. *Journal of Geophysical Research*, **93**, pp. 15467–15472, 1988.
[65] Fairall, C.W., Bradley, E.F., Rogers, D.P., Edson, J.B. & Young, G.S., Bulk parameterization of air-sea fluxes for TOGA COARE. *Journal of Geophysical Research*, **101**, pp. 3747–3764, 1996.
[66] Fairall, C.W., Bradley, E.F., Hare, J.E., Grachev, A.A. & Edson, J.B., Bulk parameterization of air-sea fluxes: updates and verification for the COARE algorithm. *Journal of Climate*, **16**, pp. 571–591, 2003.
[67] Zeng, X., Zhao, M. & Dickinson, R.E., Intercomparison of bulk aerodynamic algorithms for the computation of sea surface fluxes using TOGA COARE and TAO data. *Journal of Climate*, **11**, pp. 2628–2644, 1998.
[68] Bourassa, M.A., Vincent, D.G. & Wood, W.L., A flux parameterization including the effects of capillary waves and sea state. *Journal of the Atmospheric Sciences*, **56**, pp. 1123–1139, 1999.
[69] Wu, J., Laboratory studies of wind-wave interaction. *Journal of Fluid Mechanics*, **34**, pp. 91–112, 1968.
[70] Hasselmann, K., Barnett, T.P., Bouws, E., Carlson, H., Cartwright, D.E., Enke, K., Ewing, J.A., Gienapp, H., Hasselmann, D.E., Kruseman, P., Meerburg, A., Müller, P., Olbers, D.J., Richter, K., Sell, W. & Walden, H., Measurements of wind-wave growth and swell decay during the Joint North Sea Wave Project (JONSWAP). *Deutsche Hydrographische Zeitung*, **A8**(Suppl. 12), 95pp., 1973.
[71] Komen, G.J., Cavaleri, L., Donelan, M., Hasselmann, K., Hasselmann, S. & Janssen, P.A.E.M., *Dynamics and Modelling of Ocean Waves*, Cambridge University Press: Cambridge, 1994.
[72] Kitaigorodskii, S.A. & Volkov, Y.A., On the roughness parameter of the sea surface and the calculation of momentum flux in the near-water layer of the

atmosphere. *Izvestiya, Atmospheric and Oceanic Physics*, **1**, pp. 973–988, 1965.

[73] Donelan, M.A., The dependence of the aerodynamic drag coefficient on wave parameters. *First International Conference on Meteorology and Air-Sea Interaction of the Coastal Zone*, American Meteorological Society: Boston, pp. 381–387, 1982.

[74] Taylor, P.K. & Yelland, M.J., The dependence of sea surface roughness on the height and steepness of the waves. *Journal of Physical Oceanography*, **31**, pp. 572–590, 2000.

[75] Drennan, W.M., Taylor, P.K. & Yelland, M.J., Parameterizing the sea surface roughness. *Journal of Physical Oceanography*, **35**, pp. 835–848, 2005.

[76] Clayson, C.A., Fairall C.W. & Curry, J.A., Evaluation of turbulent fluxes at the ocean surface using surface renewal theory. *Journal of Geophysical Research*, **101**, pp. 28503–28513, 1996.

[77] Geernaert, G.L., Measurements of the angle between the wind vector and wind stress vector in the surface layer over the North Sea. *Journal of Geophysical Research*, **93**, pp. 8215–8220, 1988.

[78] Geernaert, G.L., Hansen, F., Courtney, M. & Herbers, T., Directional attributes of the ocean surface wind stress vector. *Journal of Geophysical Research*, **98**, pp. 16571–16582, 1993.

[79] Rieder, K.F., Smith, J.A. & Weller, R.A., Observed directional characteristics of the wind, wind stress and surface waves on the open ocean. *Journal of Geophysical Research*, **99**, pp. 22589–22596, 1994.

[80] Grachev, A.A., Fairall, C.W., Hare, J.E., Edson, J.B. & Miller, S.D., Wind stress vector over ocean waves. *Journal of Physical Oceanography*, **33**, pp. 2408–2429, 2003.

[81] Stewart, R.W., The wave drag of wind over water. *Journal of Fluid Mechanics*, **10**, pp. 189–194, 1961.

[82] Janssen, P.A.E.M., Wave-induced stress and the drag of air flow over sea waves. *Journal of Physical Oceanography*, **19**, pp. 745–754, 1989.

[83] Makin, V.K. & Mastenbroek, C., Impact of waves on air-sea exchange of sensible heat and momentum. *Boundary-Layer Meteorology*, **79**, pp. 279–300, 1996.

[84] Edson, J.B. & Fairall, C.W., Similarity relationships in the marine atmospheric surface layer for terms in the TKE and scalar variance budgets. *Journal of the Atmospheric Sciences*, **55**, pp. 2311–2328, 1998.

[85] Smedman, A.S., Tjernström, M. & Högström, U., The near-neutral marine atmospheric boundary layer with no surface shearing stress: a case study. *Journal of the Atmospheric Sciences*, **51**, pp. 3399–3411, 1994.

[86] Smedman, A.S., Högström, U., Bergström, H., Rutgersson, A., Kahma, K.K. & Pettersson, H., A case study of air-sea interaction during swell conditions. *Journal of Geophysical Research*, **104**, pp. 25833–25852, 1999.

[87] Kudryavtsev, V.N. & Makin, V.K., Coupled dynamics of short waves and the airflow over long surface waves. *Journal of Geophysical Research*, **107**(C12), 3209, doi:10.1029/2001JC001251, 2002.

[88] Kaimal, J.C. & Gaynor, J.E., Another look at sonic anemometry. *Boundary-Layer Meteorology*, **56**, pp. 401–410, 1991.
[89] Delahaye, J.Y., Guérin, C., Vinson, J.P., Dupuis, H., Weill, A., Branger, H., Eymard, L., Lavergnat, J. & Lachaud, G., A new shipborne microwave refractometer for estimating the evaporation flux at the sea surface. *Journal of Atmospheric and Oceanic Technology*, **18**, pp. 459–475, 2001.
[90] Sjöblom, A. & Smedman, A.S., The turbulent kinetic energy budget in the marine atmospheric surface layer. *Journal of Geophysical Research*, **107**(C10), doi:10.1029/2001JC001016, 2002.
[91] Liu, W.T., Katsaros, K.B. & Businger, J.A., Bulk parameterization of air-sea exchanges of heat and water vapor including the molecular constraints at the interface. *Journal of the Atmospheric Sciences*, **36**, pp. 1722–1735, 1979.
[92] Brutsaert, W., *Evaporation into the Atmosphere*, Reidel: Dordrecht and Boston, 1982.
[93] Donelan M.A. & Drennan, W.M., The effect of surface roughness on the fluxes of CO_2 and H_2O, manuscript in preparation, 2004.
[94] Fairall, C.W., Bradley, E.F., Godfrey, J.S., Wick, G.A., Edson, J.B. & Young, G.S., Cool-skin and warm-layer effects on sea surface temperature. *Journal of Geophysical Research*, **101**, pp. 1295–1308, 1996.
[95] Oost, W.A., Jacobs, C.M.J. & van Oort, C., Stability effects on heat and moisture fluxes at sea. *Boundary-Layer Meteorology*, **95**, pp. 271–302, 2000.
[96] Andreas, E.L., Edson, J.B., Monahan, E.C., Rouault, M.P. & Smith, S.D., The spray contribution to net evaporation from the sea: a review of recent progress. *Boundary-Layer Meteorology*, **72**, pp. 3–52, 1995.
[97] Andreas, E.L. & DeCosmo, J., The signature of sea spray in the HEXOS turbulent heat flux data. *Boundary-Layer Meteorology*, **103**, pp. 303–333, 2002.
[98] Jacobs C.M.J., Kohsiek, W. & Oost, W.A., Air-sea fluxes and transfer velocity of CO_2 over the North Sea: results from ASGAMAGE. *Tellus B*, **51**, pp. 629–641, 1999.
[99] Wanninkhof, R., Relationship between wind speed and gas exchange over the ocean. *Journal of Geophysical Research*, **97**, pp. 7373–7382, 1992.
[100] Watson, A., Upstill-Goddard, R. & Liss, P.S., Air-sea exchange in rough and stormy seas, measured by a dual tracer technique. *Nature*, **349**, pp. 145–147, 1991.
[101] Reul, N., Branger, H. & Giovanangeli, J.P., Air flow separation over unsteady breaking waves. *Physics of Fluids*, **11**, pp. 1959–1961, 1999.
[102] Wright, C.W., Walsh, E.J., Vandemark, D., Krabill, W.B., Garcia, A.W., Houston, S.H., Powell, M.D., Black, P.G. & Marks, F.D., Hurricane directional wave spectrum spatial variation in the open ocean. *Journal of Physical Oceanography*, **31**, pp. 2472–2488, 2001.

[103] Donelan, M.A., Dobson, F.W., Smith S.D. & Anderson, R.J., On the dependence of sea surface roughness on wave development. *Journal of Physical Oceanography*, **23**, pp. 2143–2149, 1993.
[104] Emanuel, K.A., Thermodynamic control of hurricane intensity. *Nature*, **401**, pp. 665–669, 1999.
[105] Powell, M.D., Vickery, P.J. & Reinhold, T.A., Reduced drag coefficient for high wind speeds in tropical cyclones. *Nature*, **422**, pp. 279–283, 2003.
[106] Andreas, E.L. & Emanuel, K.A., Effects of sea spray on tropical cyclone intensity. *Journal of the Atmospheric Sciences*, **58**, pp. 3741–3751, 2001.